Chemical Science

ROYAL SOCIETY OF CHEMISTRY

EDGE ARTICLE

View Article Online
View Journal | View Issue

Cite this: *Chem. Sci.*, 2022, **13**, 8401

All publication charges for this article have been paid for by the Royal Society of Chemistry

Unexpected molecular diversity of brown carbon formed by Maillard-like reactions in aqueous aerosols†

Shanshan Tang,[ab] Feifei Li,[bf] Jitao Lv,*[bf] Lei Liu,[cd] Guangming Wu,[ef] Yarui Wang,[bf] Wanchao Yu,[bf] Yawei Wang*[abf] and Guibin Jiang[abf]

Atmospheric brown carbon (BrC) exerts a key impact on the global radiative balance due to its light-absorbing properties. Maillard-like reactions between carbonyl and amino compounds have been identified as an important pathway for forming secondary BrC. Although optical properties have been widely studied, the molecular composition of secondary BrC generated in Maillard chemistry remains unclear, resulting in a knowledge gap to understand its formation and light-absorbing mechanism. In this study, a combination of optical spectroscopy, ^{1}H nuclear magnetic resonance (NMR), and Fourier transform ion cyclotron resonance mass spectrometry (FT-ICR MS) was employed to comprehensively characterize the chemical and light-absorbing characteristics of secondary BrC. The results indicate that both the light-absorbing and molecular characteristics of secondary BrC were highly related to the structures of their precursors. Organic amine precursors consistently result in enhanced light-absorbing capacities of BrC compared to ammonium, but have inconsistent effects on the molecular diversity of BrC. Compared to amino precursors (*i.e.*, glycine, ethylamine, propylamine, and ammonium), carbonyl precursors play a more important role in determining the molecular diversity of BrC. Different from black carbon, the light-absorbing products from Maillard-like reactions are mainly nitrogen-containing heterocycles. Unexpectedly, 35–64% of molecular formulae detected in real atmospheric samples were found in simulated Maillard reaction products, implying a potentially important contribution of Maillard chemistry to the atmospheric organic molecular pool. These results will improve our understanding of the formation and molecular diversity of BrC, and further help to manage emissions of secondary aerosol precursors.

Received 23rd May 2022
Accepted 29th June 2022

DOI: 10.1039/d2sc02857c

rsc.li/chemical-science

Introduction

Brown carbon (BrC) is defined as the light-absorbing fraction of atmospheric organic aerosols,[1] which represents an important climate forcer due to its effective absorption of solar radiation.[2] Despite significant efforts, considerable uncertainty remains in the assessment of direct radiative forcing of BrC (0.09–0.6 W m^{-2}),[3–6] due to the incomplete understanding of BrC formation and aging processes as well as its chemical composition and optical properties.

Generally, atmospheric BrC can be produced from various primary emissions (*e.g.*, biomass burning[7] and fossil fuel combustion[8]) and secondary formation,[9,10] and the latter is more complex because it involves gas-, particle- and aqueous-phase reactions through various precursors.[11] In recent years, the sources, and optical and chemical characteristics of secondary BrC have been widely studied in field and laboratory studies.[12–16] In particular, BrC produced by Maillard-like reactions between carbonyls and reduced nitrogen species (*e.g.*, organic amines and ammonium) in clouds and aqueous aerosols has attracted increasing attention,[9,10,17,18] because the related precursors are abundant in the atmosphere and the related reactions can be greatly accelerated in atmospheric aerosols. The light-absorbing capacities of BrC formed by reactions between a series of carbonyl compounds and ammonium sulfate (AS) and/or amines were evaluated, and it is confirmed that amines are considerably more effective than AS for the production of BrC on a per mole basis.[18] A recent study has reported that the single scattering albedo of a methylglyoxal

[a]*School of Environment, Hangzhou Institute for Advanced Study, University of Chinese Academy of Sciences, Hangzhou 310024, China. E-mail: ywwang@rcees.ac.cn*

[b]*State Key Laboratory of Environmental Chemistry and Eco-toxicology, Research Center for Eco-environmental Sciences, Chinese Academy of Sciences, Beijing 100085, China. E-mail: jtlv@rcees.ac.cn*

[c]*Department of Atmospheric Sciences, School of Earth Sciences, Zhejiang University, Hangzhou 310027, China*

[d]*Beihang Hangzhou Innovation Institute Yuhang, Hangzhou 310023, China*

[e]*Key Laboratory of Tibetan Environment Changes and Land Surface Processes, Institute of Tibetan Plateau Research, Chinese Academy of Sciences, Beijing 100101, China*

[f]*University of Chinese Academy of Sciences, Beijing 100049, China*

† Electronic supplementary information (ESI) available. See https://doi.org/10.1039/d2sc02857c

(MG)–amine mixture is smaller than that of a glyoxal (GX)–amine mixture and proposed that the single scattering albedo decreases with the methyl substitution of carbonyls.[10] However, the molecular composition of products formed by Maillard chemistry is highly complicated, which presents a great challenge in identifying which products contribute to the light-absorbing properties of BrC. Recently, Fourier transform ion cyclotron resonance mass spectrometry (FT-ICR MS) has been successfully used to study the molecular diversity of organic aerosols, which provides an opportunity to explore the molecular composition of products formed by atmospheric Maillard chemistry. Moreover, through the analyses of molecular composition, optical and other chemical characteristics of products from different precursors, light-absorbing products formed through Maillard chemistry can be explored at the molecular level rather than few individual compounds.

On the other hand, the applications of ultrahigh resolution mass spectrometry in the studies of organic aerosols in recent years have greatly improved our understanding on the chemical and molecular diversity of atmospheric aerosols. Atmospheric dissolved organic matter (DOM) extracted from aerosol samples from Guangzhou was characterized using FT-ICR MS. The results indicated that BrC composition was largely driven by meteorological conditions and anthropogenic activities.[19] In addition, the high molecular diversity of organic nitrogen was illuminated in urban snow by the same means.[20] However, it is difficult to distinguish the contribution of secondary processes to the molecular diversity of atmospheric organic aerosols. Although Maillard chemistry has been considered as an important pathway for the formation of BrC in atmospheric droplets, the presence of Maillard-like reaction products in real atmospheric organic aerosols has not been revealed. To improve the real Maillard-like reactions in many laboratory simulations, it is necessary to confirm how Maillard chemistry contributes to the molecular diversity of atmospheric organic aerosols. A comparison of molecules identified by FT-ICR MS between laboratory simulations and real atmospheric samples can partially answer this question, although there are some inevitable limitations.

In this study, five carbonyl and four amine compounds as precursors were combined into twelve systems to produce secondary BrC through aqueous-phase reactions. The precursor-mediated molecular composition of Maillard-like reaction products was analyzed by FT-ICR MS, and the relationships between chemical, optical, and molecular characteristics of BrC produced by Maillard-like reactions were revealed. In addition, the extensive presence of molecules produced through Maillard-like reactions in real atmospheric organic aerosols was found. The results indicate that the products of atmospheric Maillard reactions displayed unexpected molecular diversity, and their contribution to the atmospheric molecular diversities as well as their effects on atmospheric nitrogen cycles deserve more attention.

Experimental section

Chemicals

Ammonium sulfate (AS, ≥99.0%), glycine (Gly, ≥99%), ethylamine (EA, 66.0–72.0 wt% solution), propylamine (PA, ≥99%), hydroxyacetone (HA, 90%), glyoxal (GX, 40 wt% solution), methylglyoxal (MG, 40 wt% solution), and glycolaldehyde (GAld) were purchased from Sigma-Aldrich (USA). Acrolein (AC) was purchased from Aladdin (China). All chemicals were used as received without further purification. Ultrapure water (18.2 MΩ cm) was supplied by a Milli-Q water purification system.

BrC formation experiments

To simulate an intermediate case between saturated and oversaturated secondary organic aerosol particles, a solution (0.5 M) of each carbonyl compound (*i.e.*, HA, GX, MG, AC, or GAld) was mixed with 1 M AS or amine (*i.e.*, Gly, EA, or PA), respectively.[17] For each carbonyl compound-AS/Gly system, the initial pH was adjusted to 4.0. However, it was difficult to adjust the pH value of the MG-EA/PA systems before reactions, and thus, the MG-EA/PA systems are only for reference and are not compared with other systems in the following discussion. The entire reaction process was monitored using UV-Vis and fluorescence spectrophotometers. The solutions of each reactant and their reaction products were desalinated by solid-phase extraction (SPE) using Bond Elute PPL cartridges (1 g per 6 mL; Varian, Palo Alto, CA), followed by redissolving in methanol (MS grade), and drying with high purity N_2 before analysis. The product mass yield, Y (%), was calculated by weighing the dried samples. The ESI (Text S1†) provides details of the sample desalination and calculation equation of Y (%).

$PM_{2.5}$ sample collection and preparation

Field observations were carried out at the Baoding rural site (39°08′N, 115°44′E) and Jinan urban site (36°40′N, 117°03′E) during 13–27 November 2016. The sites were located on the rooftop of a three-story building (12 m a.g.l.). Detailed information about the $PM_{2.5}$ samples can be found in a previous study[21] and Table S1.† All the collected samples were stored at −20 °C for further analyses. A portion of the filter (3–17 cm^2) was used to extract BrC. The water-soluble fraction was extracted twice with 10 mL of Milli-Q water under ultrasonication for 30 min and was filtered through a syringe filter (PVDF, 0.45 μm, Durapore). The water-soluble fractions were further treated and analyzed using FT-ICR MS.

Measurement of light-absorbing and fluorescence properties of BrC

The SPE purified samples were dissolved in ultrapure water for UV-Vis spectra and total organic carbon (TOC) analyses. UV-Vis spectra were recorded on a Shimadzu UV-2600 spectrometer at 200–800 nm with a step size of 0.5 nm. TOC concentrations were measured on a Shimadzu TOC-L-CPH instrument by high-temperature catalytic oxidation. The optical properties of BrC samples were quantified by calculating the mass absorption efficiency at 365 nm (MAE_{365}, $m^2\ g^{-1}$ C) and absorption Ångström exponent (AAE).[22]

Fluorescence properties of BrC samples were characterized using a Horiba Fluoromax-4 spectrofluorometer at room temperature. Fluorescence spectra were recorded in the signal/reference (S/R) mode and calibrated by inner filter correction,

Raman normalization, and blank subtraction.[23,24] The specific equations used for the calculation of MAE_{365}, the AAE, fluorescence parameters, and corrections are described in detail in the ESI (Text S2†).

Nuclear magnetic resonance (NMR)

SPE purified BrC samples were redissolved in D_2O for ^1H NMR analysis using a Bruker-500 MHz NMR spectrometer.[25] The signals were distinguished according to the following assignments: (1) aliphatic hydrogen (H–C, 0.6–1.8 ppm); (2) unsaturated alkyl hydrogen (H–C–C=, 1.8–3.2 ppm); (3) oxygenated aliphatic hydrogen (H–C–O, 3.2–4.4 ppm); (4) aromatic hydrogen (Ar–H, 6.0–9.0 ppm).[9,26]

ESI FT-ICR MS analysis and molecular formula assignment

The SPE purified BrC samples were redissolved using a 1 : 1 (v/v) methanol/water mixture to obtain a soluble carbon concentration of ~100 mg L^{-1} and analyzed using a 15 T SolariX FT-ICR MS (Bruker, Germany) coupled with −ESI and +ESI sources. The lower and upper mass limits were set to a mass-to-charge ratio (m/z) of 120 and 928, respectively. The detailed analysis conditions are described in the ESI† following the settings utilized in previous studies.[27,28] Meanwhile, ultrapure water and reactants (*i.e.*, Gly, EA, PA, HA, GX, MG, AC, and GAld) were analyzed to represent the blank samples using the same pretreatment procedures as BrC samples. The ESI (Text S3†) provides additional details about the operation procedures.

All possible formulae for each BrC sample were identified according to stringent criteria for elemental combinations of $C_{5-50}H_{10-100}O_{0-40}N_{0-3}S_{0-2}$ using Bruker Compass Data Analysis software (version 5.0). The molecular formula assignment was performed in the range of m/z 180 to m/z 700. The requirement for the mass error between the measured and calculated masses for a given chemical formula should be less than 0.5 ppm. Molecular formulae were assigned to peaks with a signal-to-noise ratio (S/N) ≥ 6, and the elemental ratios of H/C ≤ 2.2 and O/C ≤ 1.2 were used as further restrictions. The molecular formulae of BrC samples could be divided into four compound groups according to the modified aromaticity index (AI_{mod}) and H/C: condensed polycyclic aromatics (AI_{mod} > 0.66), polyphenols (0.66 ≥ AI_{mod} > 0.5), highly unsaturated and phenolic compounds (AI_{mod} ≤ 0.5 and H/C < 1.5), and aliphatic compounds (2.0 ≥ H/C ≥ 1.5).[29] Details of the molecular parameters and the relevant equations are provided in the ESI (Text S4†).

Network analysis

Cytoscape[30] with a MetaNetter plug-in[31] was used to conduct the network analysis. The list of m/z values from BrC samples was imported into Cytoscape, and each m/z value was defined as a node. In networks, nodes are connected to each other by edges. Network analysis requires a list of m/z values as edges in MetaNetter. Except for a possible mass difference between m/z values in AS–MG, the other edges are reactants: MG for AS–MG; Gly and MG for Gly–MG (Table S2†).

Results and discussion

Effect of precursors on optical properties of secondary BrC

Light-absorbing property is an important characteristic and evaluation indicator of BrC, and thus, the light-absorbing capacity of BrC formed by different precursors was characterized first. Considering that the initial solutions exhibit almost no absorption at wavelengths of 300–600 nm, the increased absorption after the reaction is attributed to the newly generated BrC, which can also be seen from the white–yellow–brown color variation of the solutions (Fig. 1). Specifically, for AS-related reactions (*i.e.*, AS–GX, AS–MG, AS–acrolein (AC), and AS–glycolaldehyde (GAld)), all of their products show enhanced light absorbance as the reaction time increases (Fig. S1†), demonstrating the increased formation of BrC during the

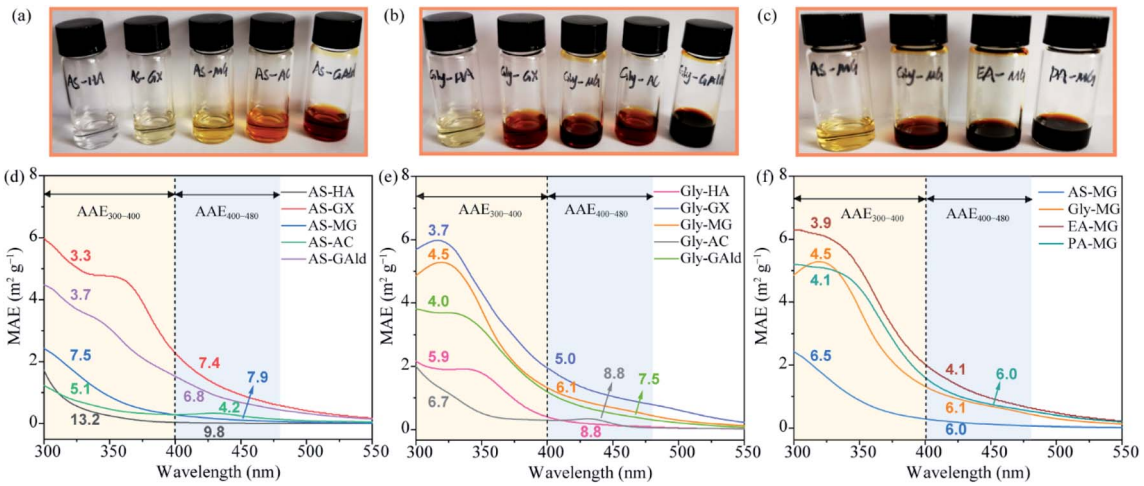

Fig. 1 Pictures of products formed by each reaction system (a–c) and their corresponding mass absorption efficiency (MAE) (d–f). The absorption Ångström exponent (AAE) at 300–400 nm and 400–480 nm wavelengths for secondary brown carbon products is also marked above or below each line in (d–f).

reaction. However, according to the absorbance variation trend during the reaction (Fig. S2a†), large differences in the formation rate of BrC exist between different reaction systems. The absorbance of the AS–AC system at 268 nm shows a rapid increase during the first 40 hours, followed by slower increases until equilibrium, while the AS–MG and AS–GAld systems have moderate reaction rates with the absorbance increasing nearly diagonally during the whole reaction time. In contrast, the AS–GX system exhibits minor absorbance variation during the reaction, which demonstrates that fewer BrC compounds are formed. After a 216 hour reaction, the AS–GAld products have the strongest light absorption over the wavelength of 200–600 nm (Fig. S3a†), indicating the importance of the carbonyl precursor in the formation of BrC through the Maillard reaction. Moreover, the BrC derived from the reaction of carbonyl compounds with organic amines (glycine (Gly), ethylamine (EA), and propylamine (PA)) displayed higher reaction rates and higher light-absorbing capacities than AS, highlighting the importance of organic amines in BrC formation. However, absorption enhancements can be barely observed for the AS–hydroxyacetone (HA) mixtures (Fig. S1†), indicating that most of the products are non-absorbent in the reaction of AS and HA. In contrast, the absorbance of the Gly–HA system at 345 nm increased by 0.09 a.u. after 120 hours, indicating that a reaction does occur between Gly and HA. It proves again that Gly has a stronger ability than AS in the formation of secondary BrC.

The absorption spectra were converted into mass absorption efficiency (MAE) using equation S2 in the ESI.† For the BrC derived from reactions between carbonyl compounds and AS, the AS–GX products exhibit the highest mass absorption efficiency at 365 nm (MAE_{365}) (Table S3†). Similarly, the Gly–GX products exhibit the highest MAE_{365} value in the BrC derived from reactions between carbonyl compounds and Gly. However, the MAE_{365} values of BrC formed by Gly are greater than those of AS, resulting from the higher electronegativity of the $-CH_2COOH$ group in Gly than that of NH_4^+ in AS. In addition, we notice that methyl substitution can decrease the MAE_{365} value, *i.e.*, AS–HA (0.15 $m^2\ g^{-1}$) < AS–GAld (2.45 $m^2\ g^{-1}$) and AS–MG (0.59 $m^2\ g^{-1}$) < AS–GX (4.50 $m^2\ g^{-1}$). In contrast, replacing the alcohol group by the carbonyl group leads to an increase in the MAE_{365} value, *i.e.*, AS–HA (0.15 $m^2\ g^{-1}$) < AS–MG (0.59 $m^2\ g^{-1}$) and AS–GAld (2.45 $m^2\ g^{-1}$) < AS–GX (4.50 $m^2\ g^{-1}$). BrC formed by MG and GX (dicarbonyls) has a larger light-absorbing capacity than HA and GAld (monocarbonyls), respectively, indicating that dicarbonyls are more important precursors in BrC formation. The absorption Ångström exponent (AAE) is used to reflect the wavelength dependence of light absorption and is commonly in the range of 2–7 or even greater up to 12 for atmospheric BrC.[32] The AAE value of each system herein was calculated at UV (300–400 nm) and visible wavelengths (400–480 nm), as shown in Fig. 1 and Table S3.† The overlapping AAE range of atmospheric and water-soluble BrC indicates that they can be regarded as a surrogate of the moderately absorbing type of BrC. According to the above results, reactions between simple carbonyl and amino (*i.e.*, Gly, EA, PA, and AS) compounds have the potential to form secondary BrC, but the reaction rates and light-absorbing properties of products are different. Many organic aerosols exhibit strong fluorescence, especially for the aqueous-phase reaction products of small carbonyl compounds with AS/amines.[9,18] Considering its high sensitivity and non-destructive analysis characteristics, fluorescence has been used recently to analyze water-soluble organics in atmospheric aerosols.[9,33,34] The fluorescence results of AS–GX and AS/Gly–AC systems herein reveal a peak at excitation/emission at 290–315 nm/370–420 nm (Fig. S5†). This region exhibits relatively shorter excitation and emission wavelengths than in a previous study.[9] Red shifts in both emission and excitation wavelengths are shown in the peak of BrC generated by Gly compared to that of AS, which indicates that products generated by Gly have larger molecular weights and higher aromaticity.

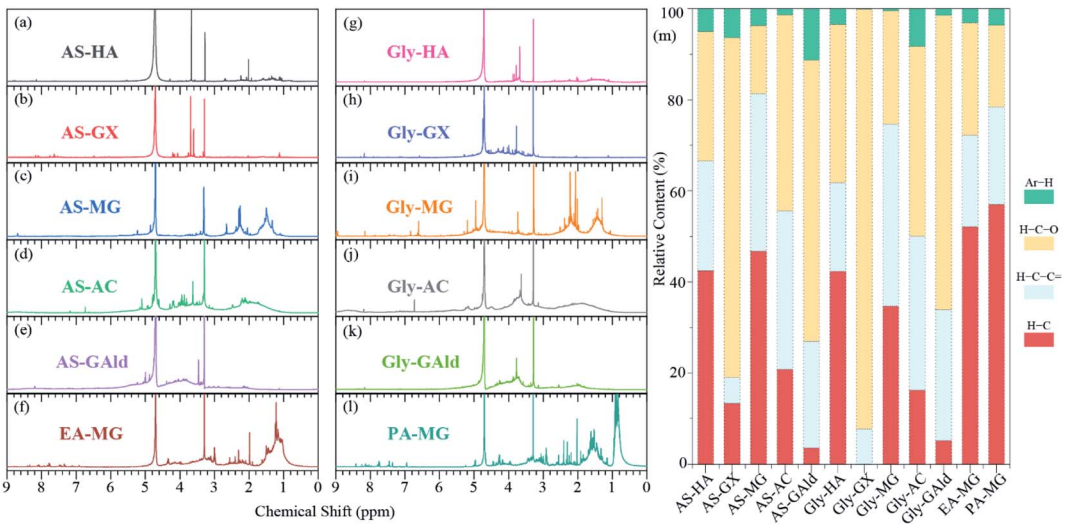

Fig. 2 ^{1}H NMR spectra of secondary brown carbon products (a–l) and the relative content of four classification groups for ^{1}H NMR spectra (m). The red, light blue, yellow, and green colors in panel (m) represent the H–C, H–C–C=, H–C–O, and Ar–H. The ^{1}H NMR spectra include a D_2O solvent peak near 4.7 ppm.

Chemical characterization of secondary BrC by NMR analysis

^{1}H NMR techniques can provide detailed structural characteristics and quantify the composition of different functional groups of secondary BrC, in particular, to offer partial validation of our major findings. As shown in Fig. 2, similar ^{1}H NMR spectra are observed for secondary BrC formed by the same carbonyl precursor with AS or amines. However, a notable difference is observed when different carbonyl compounds are used as precursors to react with AS or amines. Dividing the spectra into several key proton regions and evaluating the relative contributions of the total spectral intensity can reveal the chemical environment of protons (Fig. 2). The low amounts of the Ar–H type (6.0–9.0 ppm) for all samples studied here (Table S4†) means that the light-absorbing groups in BrC formed by Maillard reactions may be nitrogen-containing heterocycles rather than carbon-only homocyclic aromatic carbon structures. In addition, the products using HA and MG as the precursors exhibit higher amounts of the H–C type (in the range of 0.6–1.8 ppm, >30%) than the other products, possibly attributed to the existence of a methyl group in HA and MG molecular structures (Table S4†). Meanwhile, the methyl substitution in amine precursors (EA and PA) also leads to higher amounts of the H–C type (>50%). Lack of a methyl group in GX and GAld precursors causes higher amounts of the H–C–O–R type (>60%), indicating that the methyl substitution in the precursor has a great influence on the structure of BrC. The findings through NMR suggest that different precursors may exert a crucial effect on the chemical structures of secondary BrC, especially carbonyl precursors, which further supports the abovementioned findings that the precursor carbonyl compounds are more important in determining the optical properties of secondary BrC than amino precursors.

Molecular components of secondary BrC detected by ESI FT-ICR MS

To further explore the chemical composition of secondary BrC produced by different precursors at the molecular level, non-target analysis based on ESI FT-ICR MS was employed to reveal the molecular components of BrC. Unlike aqueous DOM or humic acids which contained more detected molecular formulae in negative-ion ESI (−ESI) mode, BrC produced by Maillard reactions contained a larger number of detected molecular formulae in positive-ion ESI (+ESI) mode (Table S5†). This is ascribed to the fact that products formed by Maillard reactions are rich in basic functional groups (e.g., amino) and poor in acidic functional groups (e.g., carboxyl), and are thus readily ionized in the +ESI mode.[35] More molecules with higher oxygen-containing groups (higher O/C$_w$) were detected in the −ESI mode, while molecules with higher nitrogen-containing groups were detected in the +ESI mode (Fig. S6†). In addition, more high molecular weight molecules were detected in the +ESI mode, indicating more high molecular weight molecules in Maillard reactions contained basic functional groups. The van Krevelen diagrams of assigned molecular formulae display that +ESI detects more molecules in the lower O/C region (Fig. S7 and S8†). All these results indicate that a combination of +ESI and −ESI modes is necessary to explore the molecular composition of BrC. Therefore, we recommend the usage of

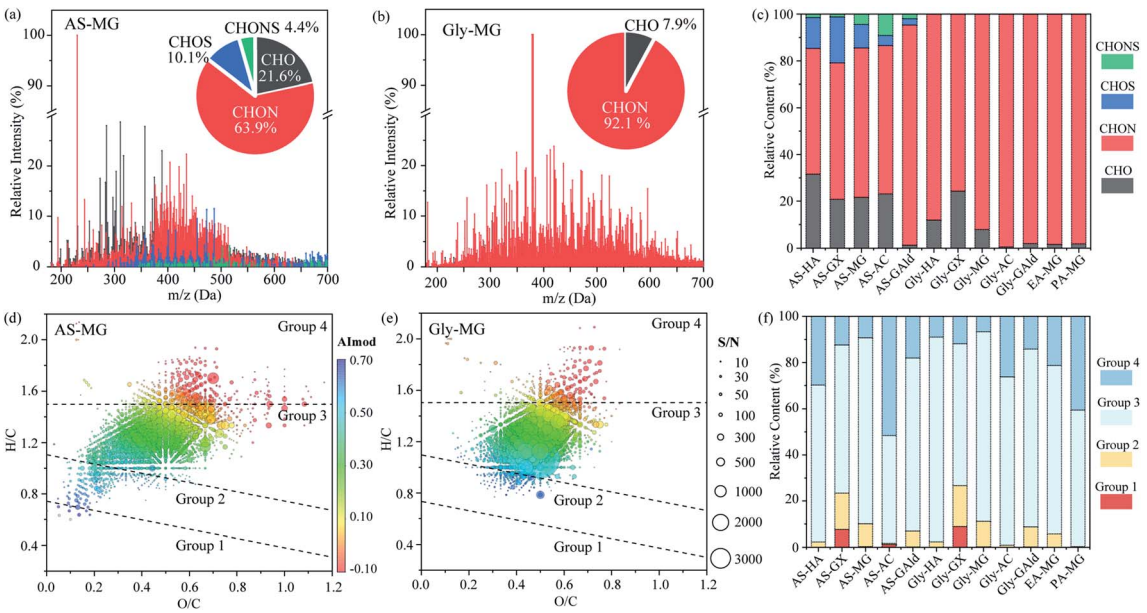

Fig. 3 Reconstructed mass spectra of BrC formed by AS–MG (a) and Gly–MG (b). Intensities were normalized to the largest peak in each spectrum (%). The inserted pie charts indicate the number distribution of the CHO, CHON, CHOS, and CHONS molecular formulae. The percentages of CHO, CHON, CHOS, and CHONS of each sample (c); van Krevelen diagrams of identified formulae in AS–MG (d) and Gly–MG (e), and the color bar represents the aromaticity index (AI$_{mod}$) and bubble size represents the signal-to-noise ratio (S/N); four groups in the van Krevelen diagram are delineated by AI$_{mod}$ and H/C cutoffs (f), Group 1: condensed polycyclic aromatics; Group 2: polyphenols; Group 3: highly unsaturated and phenolic compounds; Group 4: aliphatic compounds).

a combination of +ESI and −ESI modes to analyze BrC or water-soluble organic carbon (WSOC) extracted from atmospheric aerosols rather than a single mode.

To simplify the description and comprehensively display the molecular diversity of BrC samples, molecular formulae detected in the −ESI and +ESI modes were combined for further analyses. The overlapped molecular formulae between two modes were below 5% of the formulae identified in a single mode. The molecular formula detected in two modes may represent the same compound or different isomers, which cannot be identified by FT-ICR MS. In this respect, we adopt the most conservative strategy by considering the formula detected in two modes as a compound molecule. As shown in Fig. 3a and b, S9, and S10,† the typical FT-ICR mass spectra of secondary BrC show that the *m*/*z* values are in the range of 180–700, and the most intense ion peaks are in the range of 300–500. These values are similar to the range observed for atmospheric particles and smoke particles produced from coal combustion.[19,36] According to Table S6,† for all secondary BrC, the number of assigned molecular formulae ranges from 749 to 4323. The number of compounds in secondary BrC will be much higher than this, because the results obtained by FT-ICR MS are only based on the molecular formulae and do not consider isomeric information. It is worth noting that BrC formed by AS–HA displayed the lowest MAE_{365} value, but contained the greatest number of molecular formulae, indicating that BrC with low light-absorbing capacity did not mean it has low molecular diversity, and *vice versa*. In addition, the methyl substitution significantly increased the molecular diversity of BrC, *i.e.*, AS–HA (4323) > AS–GAld (2079) and AS–MG (2914) > AS–GX (2313). A similar characteristic is also shown by BrC produced by Gly (Table S6†). It is contrary to the results of changes in MAE_{365}, which showed that the methyl substitution in carbonyl precursors decreased the light-absorbing capacity of BrC (Table S3†). These results further indicate that the higher light-absorbing capacity of BrC does not mean it has higher molecular diversity. In other words, only a part of the compounds produced by the Maillard reaction belong to BrC, and others displayed little light-absorbing capacity. The H/C_w and O/C_w ratios are in the range of 1.21–1.57 and 0.35–0.70, with average values of 1.34 and 0.47, respectively (Table S6†). The O/C_w ratio is within the range of atmospheric aerosols (0.40–0.77)[37,38] and secondary organic aerosols (0.46–0.53),[39] whereas it is slightly greater than that of cloud water (0.37)[40] and fog water (0.43).[41] Interestingly, the products of the reaction between AS or Gly with GX (dicarbonyls) displayed a higher O/C_w ratio and $\overline{OS}c_w$ than the products of the reaction between AS or Gly with AC (monocarbonyls), which are consistent with the relative percentages of H–C–O detected by ^{1}H NMR (Fig. 2). These results indicate that BrC produced from dicarbonyl precursors has a higher oxidation state.

The identified molecular formulae can be divided into CHO, CHON, CHOS, and CHONS groups according to their elementary compositons.[42] CHON compounds account for the largest proportion (>50%) of the overall identified molecular formulae, even greater than 90% for AS–GAld, Gly–MG, Gly–AC, and Gly–GAld systems (Fig. 3c). The BrC formed by GX exhibits a lower proportion of CHON than others, which is consistent with the lower relative percentage of the H–C–C= type in the NMR results (Fig. 2). Because of the participation of amine in Maillard reactions, the proportions of CHON compounds in produced BrC are higher than most water-extractable organic matter or HULIS extracted from atmospheric particulates.[25,42] This may be an important pathway for the conversion of amino compounds into high molecular weight organic nitrogen in secondary aerosols. Moreover, the compounds detected herein were divided into four classes based on the differences in the O/C, H/C, and modified aromaticity index (AI_{mod}) values as shown in the van Krevelen diagrams (Fig. 3d and e, S11, and S12†). The detailed classification criteria are described in the Experimental section. The majority of the formulae belonged to highly unsaturated and phenolic- (Group 3) and aliphatic compounds (Group 4) (Fig. 3f), contributing to 73.30–99.67% of the total formulae (Table S8†). The proportion of nitrogen in Group 2 is above 50%, except for AS–HA and AS–AC, which proves that most of the light-absorbing compounds in BrC formed by Maillard reactions are nitrogen-containing heterocycles rather than polyphenols. This result further confirms the speculation obtained from NMR analysis (Fig. 2). Furthermore, despite the different relative percentages of each molecular group in AS and Gly, a similar trend was observed for Group 2: GX > MG > GAld > HA > AC, which is consistent with the MAE_{365} values of BrC formed by Gly, illustrating that compounds in Group 2 may play important roles in the light-absorbing of BrC, and carbonyl precursors rather than amino determine the yield of light-absorbing products in BrC.

Chemical differences between BrC generated from different precursors

To analyze the chemical difference between secondary BrC formed by different precursors, the unique common molecules in BrC with different precursors are selected using Venn diagrams (Fig. S13†). First, the effect of amino precursors on the molecular components of BrC was compared when MG was fixed as another precursor. Their shared molecules account for 4.08–7.18% (Fig. S13a†), demonstrating that amino compounds have a significant impact on BrC formation. When the same carbonyl compound is used as one of the precursors, the *m*/*z*, double bond equivalents (DBE) and carbon oxidation state ($\overline{OS}c$) values for BrC formed by AS are lower than those for BrC formed by Gly (Fig. S14†). Only 0.14–0.78% and 0.22–1.07% shared molecular formulae are detected when five carbonyl precursors reacted with AS and Gly, respectively (Fig. S13b and c†). These ratios are smaller than those when amino precursors reacted with MG, demonstrating that the carbonyl precursors are the main factors determining the chemical composition of secondary BrC instead of amino precursors (*i.e.*, Gly, EA, PA, and AS). Fig. 4a and b show the van Krevelen diagram of the unique formulae of each BrC sample generated from AS and Gly reacting with HA, GX, MG, AC, and GAld, respectively. Each BrC sample shows its distinctive H/C and O/C ranges in the van Krevelen diagram, which possibly led to the variable MAE values and fluorescent spectra of different BrC samples (discussed

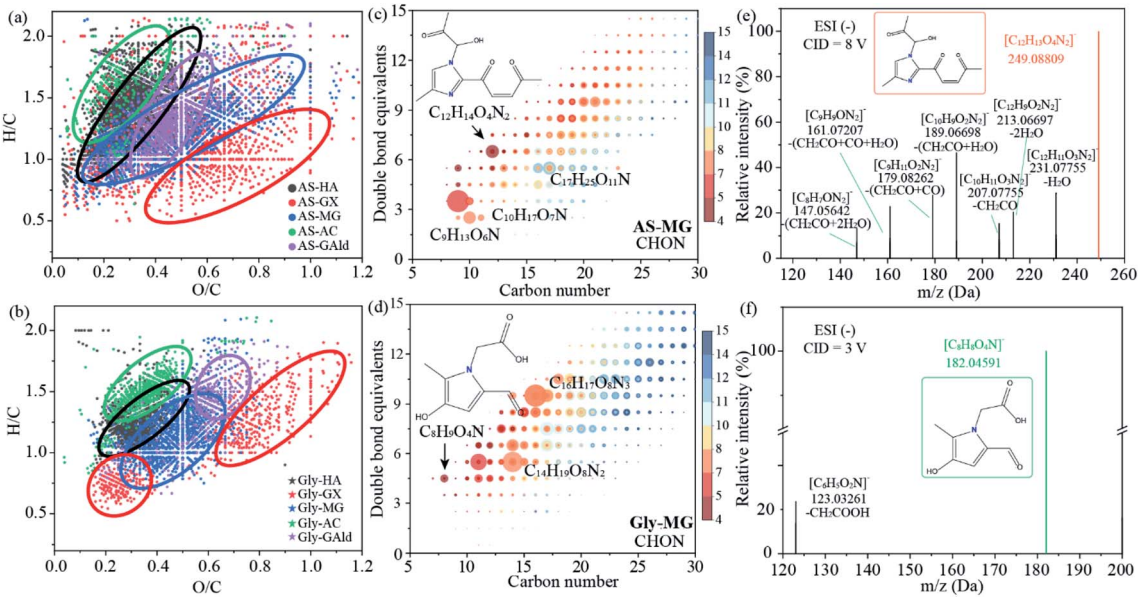

Fig. 4 The van Krevelen diagram of BrC formed by AS (a) and Gly (b) with five different carbonyl compounds. Different color indicates unique formulae detected in each sample. DBE *vs.* C number for the CHON compounds of BrC formed by AS–MG (c) and Gly–MG (d). The color bar and marker size denote the number of O atoms and the peak intensities of the compounds. The formulae for the compounds with high intensity are presented in figures. Note that the proposed structures are referenced in a previous study.[14] MS/MS fragmentation analysis for the proposed structures in FT-ICR MS (e and f).

below). AS–GX and Gly–GX products exhibit relatively lower H/C and higher O/C ratios (red circle in Fig. 4a and b) compared to other reaction products, which is consistent with their lower H–C response detected by ^{1}H NMR (Fig. 2). For the other four carbonyl compounds (*i.e.*, HA, MG, AC, and GAld), similar regions are identified between the BrC samples of the same carbonyl compound reacting with AS and Gly (Fig. 4a and b), suggesting that the molecular characteristics of secondary BrC generated by the Maillard reaction are determined more by carbonyls than by amino precursors.

Molecular components responsible for light-absorbing properties of BrC

According to previous research, the light-absorbing capacity of BrC is highly variable and strongly correlated with the molecular characteristics.[19,36,42] During the atmospheric transport, the light-absorbing properties of BrC are subject to the aging effect, and the related mechanism is extremely complex. A total of 12 samples with substantially different molecular components were obtained in this study, which provides a possibility to investigate this link. On the other hand, not all molecules are light-absorbing as discussed above, and thus it is necessary to further analyze the links between molecular characteristics and light-absorbing properties of BrC. First, MAE_{365} values are in good agreement with the results of FT-ICR MS. For example, the highest O/C_w ratio and higher proportion of polyphenols (Group 2) in secondary BrC formed by GX (dicarbonyl) support the explanation of the high MAE_{365} values. By comparison, AC, a monocarbonyl precursor, exhibits the lowest O/C_w ratio and higher amounts of aliphatic compounds (Group 4) than other precursors, corresponding to its lowest MAE_{365} value. Considering that most molecules in Group 2 are considered to contain nitrogen-containing heterocycles, they may be the main light-absorbing compounds in BrC products rather than carbon-only homocyclic aromatics. This also illustrates that chemical specificity for different carbonyl compounds in the formation of secondary BrC could lead to a different effect on the optical properties. Moreover, an FI value of <1.4 indicates that the fluorophore has higher aromaticity, while an FI value of >1.9 corresponds to lower aromaticity.[23] FI values of all samples except for the Gly–GX and Gly–AC systems herein are less than 1.4 (Table S3†), indicating that a majority of secondary BrC are formed by Maillard reactions with higher aromaticity. This finding agrees well with the high relative percentages of Group 2 in the FT-ICR MS results. A red shift in the emission and excitation wavelengths is observed in the peak of BrC generated by Gly compared with that generated by AS. It indicates that products generated by Gly exhibit higher molecular weight and higher aromaticity, which agrees well with the FT-ICR MS results as described in the above text.

Fig. S15† displays the Pearson correlation matrix of optical property parameters with chemical and molecular characteristics of BrC. A significantly positive correlation between MAE_{365} and $\overline{OS}c$ ($r = 0.73$, $p < 0.05$) is observed, suggesting that the oxidation level plays a vital role in the light-absorbing capacity of secondary BrC generated by Maillard reactions. MAE_{365} values are positively correlated with the chemical compositions related to condensed polycyclic aromatics ($r = 0.72$ and $p < 0.05$) and polyphenols ($r = 0.85$ and $p < 0.01$), confirming the dependence of the light-absorbing capacity on chemical characteristics. Moreover, the AAE value is also a significant

parameter in climate models, whereas correlations are not observed between AAE values and molecular characteristics, implying that the AAE can be affected by various factors. Therefore, we speculate that the molecular structure considerably affects the light-absorbing capacity, which provides clues for the molecular-level study of atmospheric BrC in the future. This study confirmed that the physicochemical properties of BrC are associated with their molecular composition, which improves our understanding of BrC.

The light absorption of the benzene ring is at 260 nm ($\pi \rightarrow \pi^*$ electronic transition),[43] while the nitrogen-containing heterocyclic ring is different from the benzene ring. For example, imidazole, imidazole-2-carboxaldehyde (IC), and 2,2′-biimidazole (BI) have been characterized to absorb at 207, 273, and 280 nm, respectively.[44,45] The observed UV-Vis spectra in this study revealed three major bands: ~280 nm, ~320/340 nm, and a broad band extending from 400 nm, which further prove the conclusion that light-absorbing groups in the products formed by Maillard-like reactions are nitrogen-containing heterocyclic rings rather than carbon-only homocyclic aromatics. The absorption peaks at 250–320 nm in the AS–MG mixtures are consistent with methylimidazole products (*e.g.*, 4-

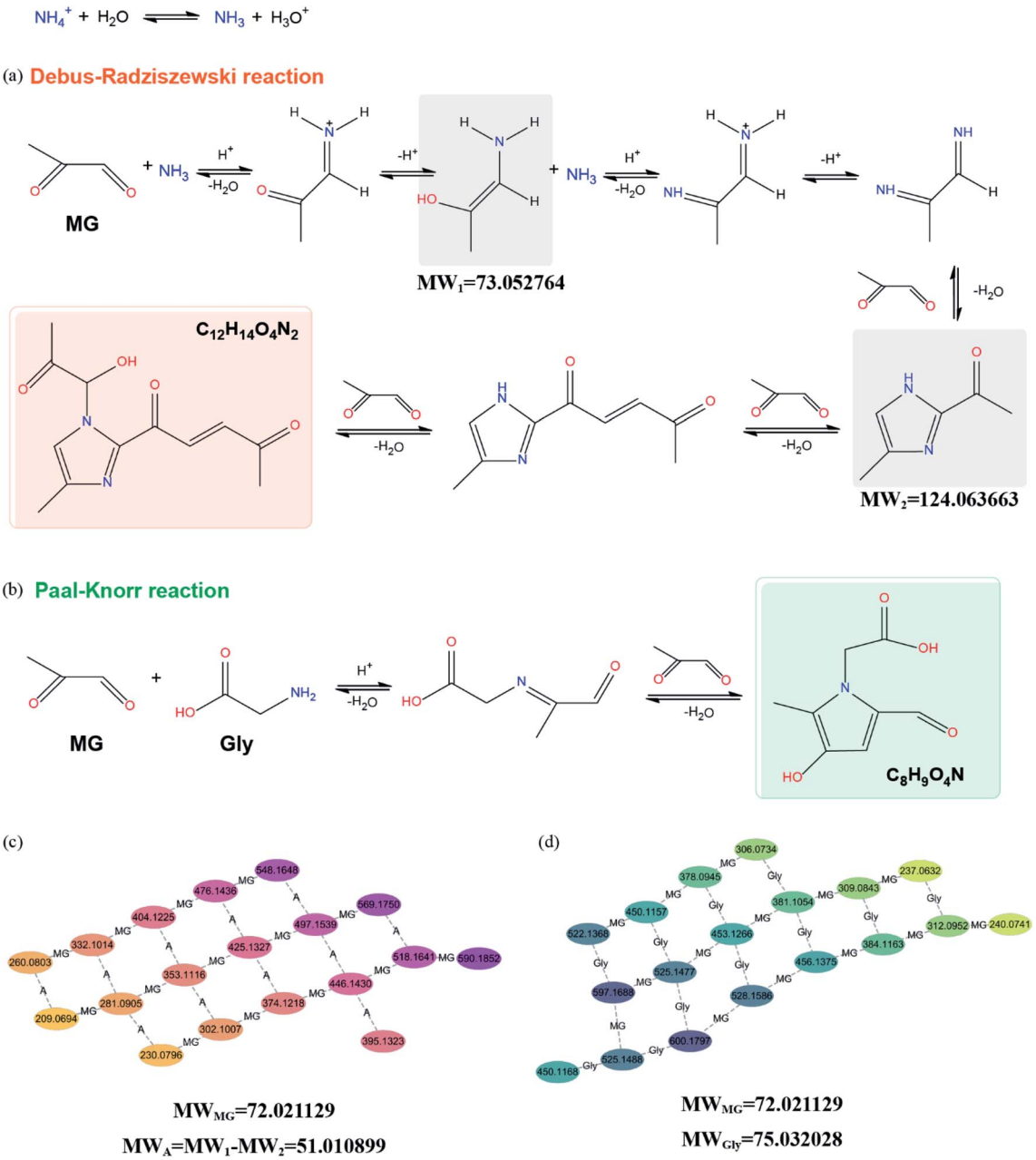

Fig. 5 Proposed reaction mechanism and molecular structures of $C_{12}H_{14}O_4N_2$ (−ESI) in AS–MG (a) and $C_8H_9O_4N$ (−ESI) in Gly–MG (b); parts of the results from a network analysis for AS–MG (c) and Gly–MG (d). Each circle within (c) and (d) represents a node which is the molecular weight (MW) value. The nodes are connected by edges which correspond to one of the chemical transformations. The complete list of chemical transformations is given in Table S8.†

methyl-2-acetylimidazole and 4-methylimidazole),[46] and the absorption peak at ~340 nm might be 1,3-diglycine-imidazole.[47] Therefore, the light-absorbing capacity of Maillard-like reaction products may be due to the formation of compounds containing the imidazole group. In addition, the FT-ICR MS results indicate that the high-intensity products detected in the AS–MG system mainly have a C number from 9 to 17 with a DBE from 3 to 7 (Fig. 4c), such as $C_9H_{13}O_6N$, $C_{10}H_{17}O_7N$, $C_{12}H_{14}O_4N_2$, and $C_{17}H_{25}O_{11}N$. As shown in Fig. 4d, the high-intensity compounds detected in the Gly–MG system have higher C numbers (12–18) and DBE (5–10), such as $C_8H_9O_4N$, $C_{14}H_{19}O_8N_2$, and $C_{16}H_{17}O_8N_3$, illustrating that most of the products from the Gly–MG system are unsaturated compounds with a high molecular weight. The C number *vs.* DBE plots of other systems are in the ESI (Fig. S16 and S17†). It is worth noting that the N-heterocyclic structures of $C_{12}H_{14}O_4N_2$ and $C_8H_9O_4N$ have been identified in the products of the dicarbonyl–imine reaction using HPLC-diode array detector (DAD)-ESI MS/MS.[14] Here, besides an accurate *m*/*z* being identified, FT-ICR MS/MS was used to detect fragment ions of $C_{12}H_{14}O_4N_2$ and $C_8H_9O_4N$ (Table S9†). No N was lost in all detected fragment ions indicating the stable structure of N-containing groups (Fig. 4e and f). Therefore, we considered that N was present in compounds as an N-heterocyclic structure as previously reported.[14] Based on the considered structures of $C_{12}H_{14}O_4N_2$ and $C_8H_9O_4N$, typical reaction pathways to form BrC are proposed in Fig. 5. The light-absorbing substances formed by the Maillard-like reaction are mainly nitrogen-containing organics with imidazole and pyrrole as the parents produced *via* the Debus–Radziszewski reaction[48] and Paal–Knorr reaction,[49,50] respectively (Fig. 5a and b). Following the above mechanism, the structures of other BrC systems are proposed tentatively based on the FT-ICR MS results (Fig. S18†). These results indicate that the light-absorbing products from Maillard-like reactions are mainly due to N-heterocycles, which are different from the black carbon structure released from primary combustion.

Molecular network analysis is a method to visualize how molecules are connected to each other by a specific mass difference. In order to explore the universality of these reaction pathways, molecular network analyses were conducted using mass data of the products of AS–MG and Gly–MG, respectively. Two mass differences were set according to the proposed reactions in Fig. 5a and b, and the edges of the network refer to the proposed transformations. The results reveal that plenty of molecular clusters were formed for each system. Fig. 5c and d show the parts of the results from a network analysis for AS–MG and Gly–MG, respectively. Molecules with an *m*/*z* between 200–600 are generated through continuous reactions, and the connection between molecules indicates that thousands of molecules are both products and reactants, which contributed to the high molecular diversity of BrC products. The statistics of edges show that carbonyl compounds are involved in a larger number of reactions (Table S2†), indicating a larger contribution of carbonyl precursors to the diversity of BrC. Maillard-like reactions are considered to be important pathways for the formation of these nitrogen heterocyclic compounds in BrC, and their contributions may be enhanced regionally if dicarbonyls and amines overlap in agricultural regions that experience persistently high amine concentrations. Future studies are encouraged to develop specific molecular markers to quantify the contribution of BrC formed by Maillard-like reactions.

Potential contribution of Maillard chemistry to the molecular diversity of atmospheric organic aerosols

In summary, 14 045 unique molecules were detected in the simulated systems in this study. Considering the coexistence of various precursors in a real atmospheric environment, the molecular composition of secondary BrC produced through Maillard chemistry would be much more complex. In order to verify whether molecular formulae in BrC formed through Maillard chemistry contributed to real atmospheric aerosols, water extracted fractions of ten $PM_{2.5}$ samples collected from rural and urban sites were analyzed by FT-ICR MS and the shared molecules in real samples and molecules obtained in simulated experiments were further extracted (selected Venn diagrams are provided in Fig. S19 and Table S1†). The results show that the number of shared molecules accounts for 35.34–64.08% of the total molecular formulae detected in real

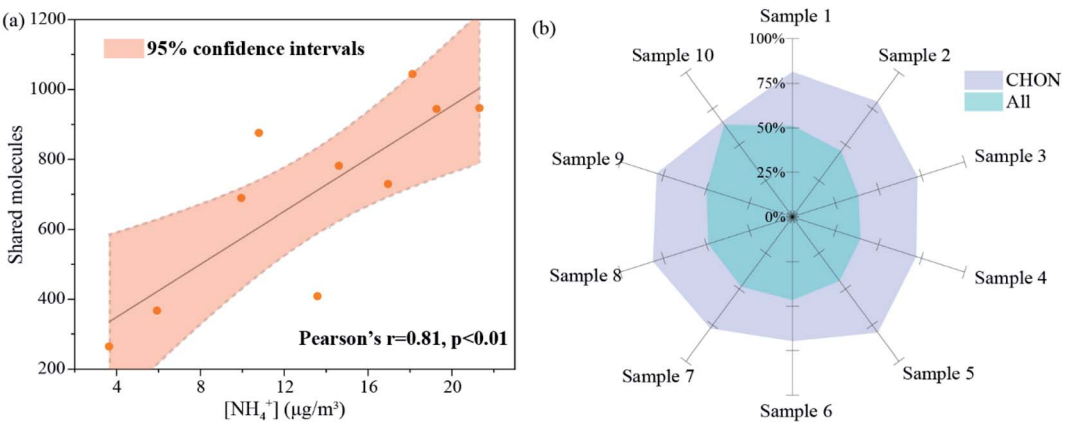

Fig. 6 Relationship between shared formulae and NH_4^+ concentrations (a); proportion of secondary BrC molecules in atmospheric samples (lake blue represents all molecules and purple represents CHON molecules) (b).

samples. Moreover, considering that NH_4^+ is an important precursor for the secondary BrC formation through Maillard-like reactions, a correlation analysis between the number of shared molecules and the concentration of atmospheric NH_4^+ was performed and a significantly positive correlation is observed ($r = 0.81$ and $p < 0.01$) (Fig. 6a). This further supports that these shared molecules detected in atmospheric aerosols are mainly derived from Maillard reactions. Although some of the molecular formulae may have different chemical structures and/or other sources, the high proportional shared molecules still indicate the extensive presence of molecules produced through Maillard-like reactions in real atmospheric organic aerosols, highlighting the potential importance of Maillard chemistry in the formation of secondary BrC. It is worth noting that a greater proportion of shared CHON formulae (66.04–81.25%) were detected in real samples (Fig. 6b), suggesting that Maillard chemistry contributed more to the atmospheric organic nitrogen molecular pool. Future studies are needed to pay more attention to the effect of Maillard chemistry on the atmospheric nitrogen cycle.

Conclusions

In this study, a combination of UV-Vis, fluorescence, ^{1}H NMR, and FT-ICR MS was employed to characterize the chemical and light-absorbing characteristics of secondary BrC produced by twelve Maillard-like reaction systems. The results indicate that both the light-absorbing and molecular characteristics were highly related to the structures of precursors. Dicarbonyls contributed more light-absorbing products than monocarbonyls, and organic amines (Gly, EA, and PA) induced the formation of stronger light-absorbing products than ammonium. The light-absorbing products from Maillard-like reactions are mainly nitrogen-containing heterocycles and some proposed strutures were provided. Carbonyl precursors rather than ammonium or amine precursors play a more important role in controlling the molecular diversity of BrC. Therefore, controlling the release of carbonyl precursors may significantly inhibit the chemical diversity of secondary BrC formed through Maillard chemistry. Furthermore, over 14 000 molecular formulae were identified in the simulated system with 35–64% of molecular formulae detected in real atmospheric samples, demonstrating that Maillard chemistry has a potentially important contribution to atmospheric organic molecules. This study provides molecular information insight into secondary BrC formed by Maillard-like reactions, which will help us to understand the formation and chemical diversity of BrC and further provide a scientific basis for managing emissions of secondary aerosol precursors.

Data availability

Experimental methods and data associated with this article, including the parameters of optical and chemical characteristics; UV-Vis spectra of secondary BrC formation; change of absorption with time; change of the fluorescence index with time and EEM spectra; ESI FT-ICR mass spectra; van Krevelen diagrams; Venn diagrams; the Pearson correlation matrix; proposed molecular structures and the plot of DBE *vs.* C number are available in the ESI.†

Author contributions

S. Tang, J. Lv and Y. W. Wang conceived and designed the study. S. Tang and F. Li performed the experiments. G. Wu and Y. R. Wang analyzed the resulting EEM data. W. Yu analyzed the mass spectral data. L. Liu, G. Wu, J. Lv and Y. W. Wang reviewed and edited the paper. Y. W. Wang and G. Jiang supervised the work. All authors contributed to the finalization of the paper.

Conflicts of interest

There are no conflicts to declare.

Acknowledgements

This research was supported by the National Natural Science Foundation of China (22021003, 22106031, and 42107108), Key Research and Development Plan of Zhejiang Province (2021C03176), Postdoctoral Science Foundation of China (2021M693319 and 2020M680695), and Postdoctoral Science Foundation of Hangzhou, China (E0BH2B039)

Notes and references

1 M. O. Andreae and A. Gelencsér, *Atmos. Chem. Phys.*, 2006, **6**, 3131–3148.
2 T. Moise, J. M. Flores and Y. Rudich, *Chem. Rev.*, 2015, **115**, 4400–4439.
3 H. Ni, R.-J. Huang, S. M. Pieber, J. C. Corbin, G. Stefenelli, V. Pospisilova, F. Klein, M. Gysel-Beer, L. Yang, U. Baltensperger, I. E. Haddad, J. G. Slowik, J. Cao, A. S. H. Prevot and U. Dusek, *Environ. Sci. Technol.*, 2021, **55**, 5701–5710.
4 S. Yue, J. Zhu, S. Chen, Q. Xie, W. Li, L. Li, H. Ren, S. Su, P. Li, H. Ma, Y. Fan, B. Cheng, L. Wu, J. Deng, W. Hu, L. Ren, L. Wei, W. Zhao, Y. Tian, X. Pan, Y. Sun, Z. Wang, F. Wu, C.-Q. Liu, H. Su, J. E. Penner, U. Pöschl, M. O. Andreae, Y. Cheng and P. Fu, *One Earth*, 2022, **5**, 293–304.
5 X. Wang, C. L. Heald, D. A. Ridley, J. P. Schwarz, J. R. Spackman, A. E. Perring, H. Coe, D. Liu and A. D. Clarke, *Atmos. Chem. Phys.*, 2014, **14**, 10989–11010.
6 R. Saleh, M. Marks, J. Heo, P. J. Adams, N. M. Donahue and A. L. Robinson, *J. Geophys. Res.: Atmos.*, 2015, **120**, 10285–10296.
7 A. P. S. Hettiyadura, V. Garcia, C. Li, C. P. West, J. Tomlin, Q. He, Y. Rudich and A. Laskin, *Environ. Sci. Technol.*, 2021, **55**, 2511–2521.
8 C. Yan, M. Zheng, C. Bosch, A. Andersson, Y. Desyaterik, A. P. Sullivan, J. L. Collett, B. Zhao, S. Wang, K. He and Ö. Gustafsson, *Sci. Rep.*, 2017, **7**, 43182.
9 L. N. Hawkins, A. N. Lemire, M. M. Galloway, A. L. Corrigan, J. J. Turley, B. M. Espelien and D. O. De Haan, *Environ. Sci. Technol.*, 2016, **50**, 7443–7452.

10 W. Marrero-Ortiz, M. Hu, Z. Du, Y. Ji, Y. Wang, S. Guo, Y. Lin, M. Gomez-Hermandez, J. Peng, Y. Li, J. Secrest, M. L. Zamora, Y. Wang, T. An and R. Zhang, *Environ. Sci. Technol.*, 2019, **53**, 117–126.
11 A. Laskin, J. Laskin and S. A. Nizkorodov, *Chem. Rev.*, 2015, **115**, 4335–4382.
12 K. Siemens, A. Morales, Q. He, C. Li, A. P. S. Hettiyadura, Y. Rudich and A. Laskin, *Environ. Sci. Technol.*, 2022, **56**, 3340–3353.
13 A. Al Nimer, L. Rocha, M. A. Rahman, S. A. Nizkorodov and H. A. Al-Abadleh, *Environ. Sci. Technol.*, 2019, **53**, 6708–6717.
14 C. J. Kampf, A. Filippi, C. Zuth, T. Hoffmann and T. Opatz, *Phys. Chem. Chem. Phys.*, 2016, **18**, 18353–18364.
15 R.-J. Huang, L. Yang, J. Shen, W. Yuan, Y. Gong, H. Ni, J. Duan, J. Yan, H. Huang, Q. You and Y. J. Li, *Environ. Sci. Technol. Lett.*, 2021, **9**, 102–111.
16 C. Yan, M. Zheng, Y. Desyaterik, A. P. Sullivan, Y. Wu and J. L. Collett, Jr., *J. Geophys. Res.: Atmos.*, 2020, **125**, e2019JD032018.
17 P. Lin, J. Laskin, S. A. Nizkorodov and A. Laskin, *Environ. Sci. Technol.*, 2015, **49**, 14257–14266.
18 M. H. Powelson, B. M. Espelien, L. N. Hawkins, M. M. Galloway and D. O. De Haan, *Environ. Sci. Technol.*, 2014, **48**, 985–993.
19 H. Jiang, J. Li, R. Sun, C. Tian, J. Tang, B. Jiang, Y. Liao, C.-E. Chen and G. Zhang, *Environ. Sci. Technol.*, 2021, **55**, 10268–10279.
20 S. Su, Q. Xie, Y. Lang, D. Cao, Y. Xu, J. Chen, S. Chen, W. Hu, Y. Qi, X. Pan, Y. Sun, Z. Wang, C.-Q. Liu, G. Jiang and P. Fu, *Environ. Sci. Technol.*, 2021, **55**, 4344–4356.
21 L. Liu, J. Zhang, Y. Zhang, Y. Wang, L. Xu, Q. Yuan, D. Liu, Y. Sun, P. Fu, Z. Shi and W. Li, *Atmos. Chem. Phys.*, 2021, **21**, 2251–2265.
22 B. You, S. Li, N. T. Tsona, J. Li, L. Xu, Z. Yang, S. Cheng, Q. Chen, C. George, M. Ge and L. Du, *ACS Earth Space Chem.*, 2020, **4**, 631–640.
23 G. Wu, P. Fu, K. Ram, J. Song, Q. Chen, K. Kawamura, X. Wan, S. Kang, X. Wang, A. Laskin and Z. Cong, *Environ. Pollut.*, 2021, **268**, 115906.
24 K. R. Murphy, C. A. Stedmon, D. Graeber and R. Bro, *Anal. Methods*, 2013, **5**, 6557–6566.
25 R. Han, J. Lv, L. Luo, B. Wen and S. Zhang, *Environ. Chem.*, 2019, **16**, 92–100.
26 A. S. Willoughby, A. S. Wozniak and P. G. Hatcher, *Atmosphere*, 2016, **7**, 79.
27 Z. Wang, J. Lv, S. Zhang, P. Christie and S. Zhang, *Environ. Sci. Technol.*, 2021, **55**, 1769–1778.
28 J. Lv, R. Han, Z. Huang, L. Luo, D. Cao and S. Zhang, *ACS Earth Space Chem.*, 2018, **2**, 330–339.
29 J. Lv, Z. Huang, P. Christie and S. Zhang, *ACS Earth Space Chem.*, 2020, **4**, 1913–1919.
30 M. E. Smoot, K. Ono, J. Ruscheinski, P.-L. Wang and T. Ideker, *Bioinformatics*, 2011, **27**, 431–432.
31 F. Jourdan, R. Breitling, M. P. Barrett and D. Gilbert, *Bioinformatics*, 2008, **24**, 143–145.
32 R.-J. Huang, L. Yang, J. Shen, W. Yuan, Y. Gong, J. Guo, W. Cao, J. Duan, H. Ni, C. Zhu, W. Dai, Y. Li, Y. Chen, Q. Chen, Y. Wu, R. Zhang, U. Dusek, C. O'Dowd and T. Hoffmann, *Environ. Sci. Technol.*, 2020, **54**, 7836–7847.
33 Q. Chen, M. Wang, Y. Wang, L. Zhang, Y. Li and Y. Han, *Environ. Sci. Technol.*, 2019, **53**, 8574–8584.
34 G. Wu, K. Ram, P. Fu, W. Wang, Y. Zhang, X. Liu, E. A. Stone, B. B. Pradhan, P. M. Dangol, A. K. Panday, X. Wan, Z. Bai, S. Kang, Q. Zhang and Z. Cong, *Environ. Sci. Technol.*, 2019, **53**, 3471–3479.
35 P. Lin, A. G. Rincon, M. Kalberer and J. Z. Yu, *Environ. Sci. Technol.*, 2012, **46**, 7454–7462.
36 J. Song, M. Li, X. Fan, C. Zou, M. Zhu, B. Jiang, Z. Yu, W. Jia, Y. Liao and P. a. Peng, *Environ. Sci. Technol.*, 2019, **53**, 13607–13617.
37 I. Kourtchev, S. Fuller, J. Aalto, T. M. Ruuskanen, M. W. McLeod, W. Maenhaut, R. Jones, M. Kulmala and M. Kalberer, *Environ. Sci. Technol.*, 2013, **47**, 4069–4079.
38 K. R. Daellenbach, I. Kourtchev, A. L. Vogel, E. A. Bruns, J. Jiang, T. Petäjä, J. L. Jaffrezo, S. Aksoyoglu, M. Kalberer, U. Baltensperger, I. El Haddad and A. S. H. Prévôt, *Atmos. Chem. Phys.*, 2019, **19**, 5973–5991.
39 A. P. Bateman, J. Laskin, A. Laskin and S. A. Nizkorodov, *Environ. Sci. Technol.*, 2012, **46**, 8315–8324.
40 A. Bianco, L. Deguillaume, M. Vaïtilingom, E. Nicol, J.-L. Baray, N. Chaumerliac and M. Bridoux, *Environ. Sci. Technol.*, 2018, **52**, 10275–10285.
41 L. R. Mazzoleni, B. M. Ehrmann, X. Shen, A. G. Marshall and J. L. Collett, *Environ. Sci. Technol.*, 2010, **44**, 3690–3697.
42 J. Tang, J. Li, T. Su, Y. Han, Y. Mo, H. Jiang, M. Cui, B. Jiang, Y. Chen, J. Tang, J. Song, P. a. Peng and G. Zhang, *Atmos. Chem. Phys.*, 2020, **20**, 2513–2532.
43 S. S. Tang, F. H. Li, N. T. Tsona, C. Y. Lu, X. F. Wang and L. Du, *ACS Earth Space Chem.*, 2020, **4**, 862–872.
44 G. Yu, A. R. Bayer, M. M. Galloway, K. J. Korshavn, C. G. Fry and F. N. Keutsch, *Environ. Sci. Technol.*, 2011, **45**, 6336–6342.
45 C. J. Kampf, R. Jakob and T. Hoffmann, *Atmos. Chem. Phys.*, 2012, **12**, 6323–6333.
46 D. O. De Haan, L. N. Hawkins, J. A. Kononenko, J. J. Turley, A. L. Corrigan, M. A. Tolbert and J. L. Jimenez, *Environ. Sci. Technol.*, 2011, **45**, 984–991.
47 Y. Gao and Y. Zhang, *Spectrochim. Acta, Part A*, 2019, **215**, 112–121.
48 A. Engelhardt, *J. Prakt. Chem.*, 1858, **75**, 373–375.
49 C. Paal, *Ber. Dtsch. Chem. Ges.*, 1884, **17**, 2756–2767.
50 L. Knorr, *Ber. Dtsch. Chem. Ges.*, 1884, **17**, 2863–2870.